*Graphical Abstract (for review)

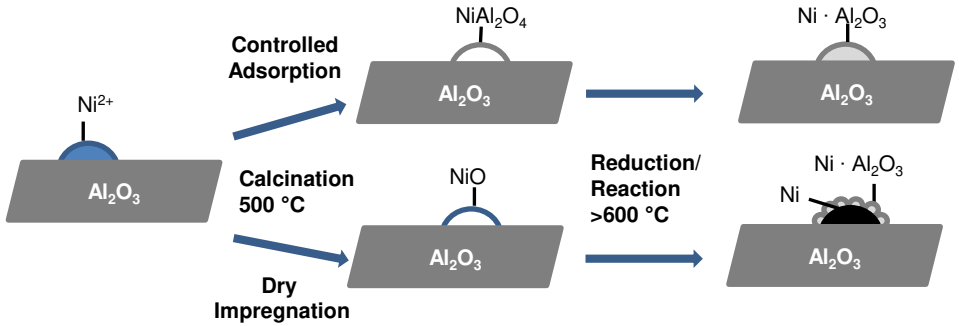

Effect of Metal Support Interactions in Ni/Al_2O_3 Catalysts with Low Metal Loading for Methane Dry Reforming

Jessica L. Ewbank,[a,b] Libor Kovarik,[c] Fatoumata Z. Diallo,[a] Carsten Sievers[a,b*]

[a] School of Chemical & Biomolecular Engineering, Georgia Institute of Technology, Atlanta, GA 30332

[b] Renewable Bioproducts Institute, Georgia Institute of Technology, Atlanta, GA 30332

[c] Pacific Northwest National Laboratory, Environmental Molecular Sciences Laboratory, Richland, WA 99352

* Phone: +1-404-385-7685, Fax: +1-404-894-2866, Email: carsten.sievers@chbe.gatech.edu

Abstract

Nickel catalysts prepared by a variety of different methods are commonly used for reforming reactions such as methane dry reforming. Two preparation methods, controlled adsorption and dry impregnation, are implemented to explore the effect of preparation method on the formation of active sites on alumina supported nickel catalysts. By varying only the preparation method, comparison of catalysts that differ primarily in metal support interactions, strong metal support interaction (controlled adsorption) and weak metal support interactions (dry impregnation), are obtained. For controlled adsorption, optimal synthesis conditions are identified using point of zero charge measurements, pH-precipitation experiments, and adsorption isotherms. Using these conditions, a catalyst with a higher dispersion and strong metal support interactions is prepared. Physicochemical characterization by N_2 physisorption, H_2 chemisorption, temperature programmed reduction (TPR), transmission electron microscopy (TEM), and environmental TEM (ETEM) shows that the types of nickel sites formed strongly depend on the synthesis method. Methane dry reforming reactivity studies show stable catalytic performance for at least 9 h and provide additional insight into the types of active centers present. After reductive pretreatment, the nickel catalyst prepared by dry impregnation is found to primarily have nickel present as a surface $NiAl_2O_4$. In contrast, the active centers for the nickel catalyst prepared by controlled adsorption consist of nickel particles that are encapsulated by a nickel aluminate layer with 1-2 nm in thickness. Combustion analysis and XPS of spent catalysts reveal different amounts and nature of carbonaceous deposits as a function of the synthesis method.

Keywords: Rational Synthesis, Nickel, Alumina, Adsorption, Metal Support Interactions

1 Introduction

Syngas is an extremely important commodity in the petroleum and chemical industry.[1] Methane steam reforming is the most common industrial route for the production of syngas. However, it provides limited yields of CO typically resulting in H_2/CO ratios between 3 - 16,[2] which are unsuitable for the production of fuels and chemicals by Fischer-Tropsch and methanol synthesis.[1] The production of syngas by methane dry reforming has attracted much attention for several reasons: the increased interest in the effective utilization of the greenhouse gas carbon dioxide, a possible way to utilize methane and carbon dioxide resulting from anaerobic digestion of biomass, and syngas production with a hydrogen to carbon monoxide ratio near one.[3, 4]

Nickel catalysts supported on γ-Al_2O_3 have been shown to be effective for methane dry reforming, steam reforming of methane and heavy hydrocarbons, hydrogenation reactions, hydrogenolysis, and amination reactions.[5-7] The exact nature of nickel species on the γ-Al_2O_3 surface affects the activity and selectivity during methane dry reforming, and identification of the different types of nickel species has been the focus of numerous studies.[2, 8-25]

The nature of nickel species will depend on the preparation method,[11, 14, 16, 17, 19] the weight loading,[11, 12, 16, 18-20] the morphology of the support,[9, 13, 15, 19] and the calcination temperature.[8, 12, 13, 15, 17, 18] Additionally, the speciation of nickel can change during the reduction of the catalyst or upon exposure to reaction conditions.

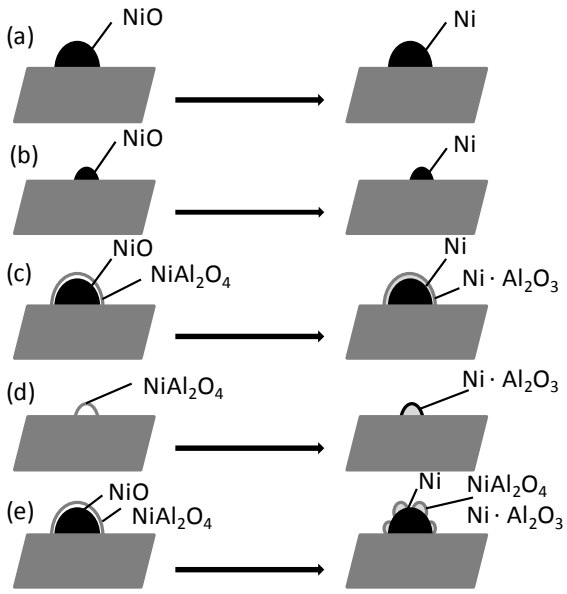

Figure 1 – Proposed models for the nickel-alumina structure after calcination (left) and after reduction (right). (a) large free NiO particles[19] (b) small free NiO particles[19] (c) large $NiAl_2O_4$ (fixed NiO) particles [19] (d) small $NiAl_2O_4$ (fixed NiO) particles[19] (e) alternative picture for the structure of large $NiAl_2O_4$ (fixed NiO) particles after reduction. [18]

Several of the commonly proposed nickel surface species are shown in Figure 1. Zielenski studied NiO/Al_2O_3 prepared by impregnation and found that NiO exists in two forms, free (Figure 1 a,b) and fixed (Figure 1 c,d).[19] Free refers to nickel that exists on the catalyst surface as nickel oxide. The occurrence of fixed nickel oxide is related to a chemical reaction between alumina and nickel oxide forming stoichiometric and non-stoichiometric nickel aluminate ($NiAl_2O_4$). It was proposed that at oxidation above 500 °C NiO particles are covered by $NiAl_2O_4$ and in the case of small fixed NiO particles, nickel forms surface $NiAl_2O_4$ (Figure 1c,d respectively).[19] Lamber et al. studied nickel alumina catalysts prepared by impregnation and coprecipitation.[13, 26] TEM studies showed that after reduction in hydrogen, metallic nickel crystallites were covered by porous aluminate shells (Figure 1e). In the case of coprecipitated catalysts used in Lambers' study, it was said that the high stability to sintering was

due to $NiAl_2O_4$ covering fixed NiO particles, in agreement with the results of Zielenski.[19, 26] Salgagre also found for nickel alumina catalysts prepared by impregnation that catalytically active nickel existed either as naked crystallites or as encapsulated nickel inside porous non-stoichiometric aluminate shells.[18]

Supported metal catalysts with low weight loading of the metal component have the desirable combination of effective metal utilization and reduced formation of carbonaceous deposits.[27] Nickel supported on alumina is reported to have higher activity than nickel supported on other oxides, and this is an indication that metal support interactions crucially influence the catalytic performance of nickel catalysts.[7] However, one of the main problems with Ni/Al_2O_3 catalysts with low nickel content is the formation of supposedly inactive nickel aluminate. In the literature, several common critical points with regards to the types of nickel species present on the alumina surface were identified: Oxidation at 500 °C was said to form stoichiometric and nonstoichiometric nickel aluminates,[13] and nickel loadings below 1 wt% were said to produce only surface $NiAl_2O_4$.[11, 20] In case of slightly higher weight loading (such as 2 wt%), different types of active sites ($NiAl_2O_4$ and NiO) are expected to be present.

To gain insight into the types and catalytic performance of nickel sites as a function of the preparation method, samples are prepared by two methods in this study: controlled adsorption and dry impregnation. Synthesis of a nickel catalyst by controlled adsorption of Ni^{2+} was inspired by the rational synthesis method strong electrostatic adsorption (SEA).[28-30] In SEA, the surface charge of the metal oxide support is exploited to maximize metal-support interactions. The point of zero charge (PZC) of a metal oxide support is the point at which the support surface is neutrally charged. At pH values above the PZC of the metal oxide, the surface is deprotonated (negatively charged), and cationic species can be electrostatically adsorbed. At

pH values below the PZC, the surface is protonated (positively charged), and anionic species can be electrostatically adsorbed. In this study, nickel nitrate (Ni^{2+}) is used as metal precursor. Therefore, alkaline conditions are used to adsorb the metal cations on the support. In the case of dry impregnation, the pores of the support are filled with a volume of aqueous precursor solution that is equal to the pore volume, and deposition of Ni^{2+} on the surface occurs during drying and calcination.[31] Nickel catalysts of 2wt% Ni are prepared, and the samples are calcined at 500 °C to explore the possibility of the formation of nickel oxide and stoichiometric/non-stoichiometric nickel aluminates. By varying only the preparation method between the two samples, valuable insight is gained on the types of active nickel sites present on nickel catalysts as a function of metal support interactions during the synthesis. Calcined catalyst samples are characterized by N_2 physisorption, elemental analysis, H_2 chemisorption, TPR, TEM/ETEM, and methane dry reforming reactivity studies. Methane dry reforming is carried out at 700 °C using a stoichiometric feed of methane and carbon dioxide for 9 h. Spent catalysts are characterized by combustion analysis and XPS.

2 Materials and Methods

1.2.1 Materials

Aluminum oxide, γ-phase, 99.97% metals basis from Alpha Aesar (surface area 80 – 120m^2/g) and $Ni(NO_3)_2$ (99.999% trace metals basis) from Aldrich were used as received. HCl and NH_4OH (A.C.S. reagent grade) from Sigma were used as pH adjustors in pH precipitation studies, adsorption isotherms, and catalyst synthesis. Deionized water was used throughout this study. Methane (U.H.P.) and Carbon Dioxide (Research Grade) utilized in reactivity studies were obtained from Airgas and used without further purification.

2.2 Controlled Adsorption (CA) Synthesis Optimization

2.2.1 Point of Zero Charge (PZC)

To determine the point of zero charge (PZC) of the γ–Al_2O_3 support, aqueous solutions with pH values ranging from 0.5 to 13 were prepared using HCl or NH_4OH. Alumina was contacted with the solutions using a mass of alumina that corresponded to a surface loading (S.L.) of 1000 m^2/L. The solutions were then shaken for one hour, and the final pH was then measured. A glass bodied Thermo Scientific Orion pH probe (9102BNWP) was employed for all pH measurements. The pH meter was calibrated using standard buffer solutions at the beginning of every experiment. The experiments were conducted using 50 mL polypropylene bottles at room temperature.

2.2.2 pH Precipitation Studies

Aqueous solutions with pH values ranging from 5.5 to 13 were prepared using NH_4OH at room temperature where 5.5 is the pH of laboratory deionized water. For each measurement, 200 ppm nickel (as nickel nitrate hexahydrate) was added to the solutions. The solutions were shaken for one hour, and the final pH was determined. Any sign of bulk precipitation (and its color) at a given pH value was noted.

2.2.3 Precursor Adsorption as a Function pH

Solutions with pH values ranging from 5.5 to 13 were prepared using NH_4OH. $Ni(NO_3)_2$ was dissolved in water to obtain a solution with a concentration of 200 ppm. The solution was allowed to equilibrate for one hour. The pH of the resulting solutions was then re-adjusted to its desired value, and the support was contacted at a surface loading of 1000 m^2/L for 40 mL of total

solution. Before contact with the support, a 2 mL sample was taken and filtered using 0.45 μm nylon syringe filters. $Ni(NO_3)_2$ and the support were shaken for one hour. A 4 mL sample was taken and filtered. A sample was also taken after 24 hours of shaking. The filtered samples were diluted and analyzed for Ni^{2+} and Al^{3+} by ICP-OES (Perkin Elmer Optima 3000 DV). Negligible deposition occurred between the 1 and 24 h time points. The aluminum concentration was found to be lower than 10 ppm in all experiments.

2.3 Catalyst Preparation

2.3.1 Controlled Adsorption (CA)

For catalysts prepared by CA, the desired amount of precursor was added to a solution, allowed to age, and the pH was adjusted to the value that corresponds to maximum adsorption. From pH- precipitation and adsorption isotherm measurements (*vide infra*) the optimum synthesis pH was found to be at a pH of 9.5 using NH_4OH. The metal solution was allowed to equilibrate for 1h at a pH of 9.5 and then re-adjusted to the desired value. The support was then contacted with the solution and shaken for 1 hour. The catalyst was filtered and washed twice with deionized water. Samples were taken and analyzed by ICP before and after contact with the support to ensure complete deposition had been attained. The 2 wt% Ni/Al_2O_3 catalyst prepared in this manner will henceforth be designated 2NiCA.

2.3.2 Dry Impregnation (DI)

The weight loading for catalysts prepared by dry impregnation was chosen to be the same as the 2NiCA catalyst. The desired amount of complex was dissolved in a volume of water that corresponded to the pore volume of the support as determined by nitrogen physisorption. The

precursor solution was added to the support and stirred for 1 h at room temperature. The 2 wt% Ni/Al_2O_3 catalysts prepared in this manner will henceforth be designated 2NiDI.

2.3.3 Calcination

Precursor loaded supports were dried briefly in an oven at 110 °C prior to calcination. 2NiCA and 2NiDI samples were heated to 500 °C at a heating rate of 5 °C/min and held for 3 h. Zero air generated using a zero air generator (VWR, 26000-020) produced UHP air with a purity level below 0.05 ppm total hydrocarbon content from the compressed air supply.

2.4 Characterization

2.4.1 Nitrogen Physisorption

Prior to N_2 physisorption, the samples were outgassed for 3 h under vacuum at 300 °C. N_2 adsorption/desorption isotherms at -196 °C were measured for calcined catalysts using Micromeritics ASAP 2020 and approximately 0.5 g of sample. The surface area was calculated using the BET method [32] and the pore size and volume using the BJH method applied to the desorption branch of the adsorption isotherm. Typically, application of the BET equation to the N_2 physisorption results produces surface area measurements within 3%.

2.4.2 Elemental Analysis

The nickel content was determined externally by Galbraith laboratories for the 2NiDI and 2NiCA samples. HF digestion was used to ensure the support was dissolved completely before analysis by ICP-OES.

2.4.3 Temperature Programmed Reduction

Temperature programmed reduction was carried out using Micromeritics ASAP 2920 equipped with a TCD detector, a reference chamber, and a cold trap. The cold trap contained a mixture of dry ice and isopropyl alcohol and ensured water did not affect the TCD signal. The concentration of the reducing gas was a 10% H_2/Ar. A flowrate of 50 mL/min and approximately 45 mg of catalyst was used in all experiments. The temperature was ramped from 25 °C to 1000 °C at 5 °C/min. In a modified TPR experiment the 2NiCA sample was pretreated at 700 °C (with a heating rate of 5 °C/min) in helium for 30 minutes. The sample was then cooled to 40 °C, and the TPR experiment was performed as described above.

2.4.4 H_2 Chemisorption

Metal dispersion was analyzed by hydrogen chemisorption using a Micromeritics Chemisorb 2750. Each experiment was performed with approximately 0.4 g of catalyst. The sample was first evacuated at 110 °C for 60 min to remove ambient gases. The temperature was ramped from 110 °C to 600 °C at 2 °C/min and held at 600 °C for 8 h. The sample was then cooled to 550 °C and evacuated for 16 h to remove residual hydrogen. Finally, the sample was cooled to 25 °C, and H_2 gas was dosed in order to perform the chemisorptions analysis. Two isotherm measurements were performed and the metal surface area was calculated using H/M ratio of 1.[8]

2.4.5 Scanning Transmission Electron Microscopy

Scanning Transmission electron microscopy (STEM) was performed with a FEI Titan 80-300 operated at 300 kV and equipped with CEOS GmbH double-hexapole aberration corrector for the probe forming lens, allowing formation of sub Ångstrom probe. The images were

recorded on a High Angle Annular Dark Field detector with a detection angle that is 3 times higher than the convergence angle. The samples for TEM observations were prepared by dispersing a dry powder on a lacey-carbon coated 200 mesh Cu TEM grids, and the as prepared grids were immediately loaded into the TEM airlock to minimize exposure to atmospheric O_2.

2.4.6 Environmental Transmission Electron Microscopy

The in-situ microscopic observations were performed with an aberration corrected Environmental Titan 80-300. The microscope is equipped with CEOS aberration corrector for the image-forming lens, which allows imaging with sub-Ångstrom resolution. The images presented in this work were acquired with Gatan's Ultra-Scan 1000S CCD camera (2048x2048), and the acquisition was performed in Digital Micrograph (DM). The gas flow entering the ETEM was controlled with a custom-built gas control unit, which utilizes Alicat^R Mass Flow Controllers (MFC) to control the composition of the gasses. Heating of the TEM samples was done with MEMS (micro-electro-mechanical systems) Aduro Protochips heating holder. Each heating chip consists of thin SiN membrane that is resistively heated based on factory calibrations. The heating currents were calibrated for vacuum conditions, and it should be noted that in the ETEM due to presence of gasses, the actual temperature is expected to be lower than the set point due to the cooling capacity of the gases.

2.4.7 X-ray Photoelectron Spectroscopy

XPS was performed on spent catalysts using a Thermo K-Alpa instrument. The instrument is equipped with a monochromatic small-spot X-ray source and a 180° double focusing hemispherical analyzer with a 128-channel detector. Spectra were obtained using an aluminum anode Al Kα ($h\nu$ = 1486.6 eV). The background pressure was 4.9×10^{-8} bar and 4×10^{-7} bar argon during measurement because of the charge compensation dual beam source,

which was used to prevent sample charging. Binding energies were referenced to the sample stage, which contains built in calibration standards of copper, silver, and gold.

2.4.8 Combustion Analysis

The C, H, and N content of spent catalysts was analyzed externally by combustion analysis at Gailbraith laboratories.

2.5 Reactivity Studies

Methane dry reforming reactions were performed in a quartz reactor that contained a 75 – 90 μm frit using 200 mg of catalyst. A stoichiometric mixture of methane and carbon dioxide was employed at a space velocity of 22,000 h^{-1}. Catalyst samples were pre-reduced in-situ at 600 °C for two hours in 20% H_2/N_2. The reaction temperature was 700 °C, and the pressure was approximately 1.5 atm. Product gas was sampled at 20 minute intervals using an online Bruker 450-GC refinery gas analyzer (RGA) that is equipped with two TCD detectors and a FID. One TCD was used for analysis of permanent gas mixtures, including methane, and the FID channel was used in this study to confirm of methane concentration from the first TCD. The second TCD is used for analysis of hydrogen.

3 Results

3.1 Synthesis of 2 wt% Ni/Al_2O_3 by Controlled Adsorption (2NiCA)

Controlling the adsorption of nickel on γ-Al_2O_3 will allow for direct comparison of the effect of metal support interactions on low weight loading nickel alumina catalysts. Three experiments were performed to optimize the adsorption of nickel on γ-Al_2O_3: a point of zero

charge (PZC) measurement, a pH precipitation study, and an adsorption isotherm. The PZC of the batch of alumina used in our experiments was previously found to be at a pH of approximately 7.7.[33] This means to adsorb cationic complexes the pH of the impregnating solution should be sufficiently above PZC, so that the surface can be deprotonated (negatively charged). This is problematic for adsorption of Ni^{2+}, which precipitates in alkaline solutions. To investigate the stability of the cationic complex in aqueous alkaline solutions, pH precipitation studies were conducted. It was found that the metal precursor solution shifted the pH of the mixture due to equilibration of the various types of ionic species in solution (e.g. $Ni(H_2O)_6^{2+}$, $Ni(OH)_2(s)$, and $Ni(H_2O)_{6-n}(NH_3)_n^{2+}$). This shift must be corrected before the adsorption steps of the synthesis procedure. Additionally, in the presence of NH_4OH, Ni^{2+} was found to precipitate between initial pH values of 10 and 11. Above a pH of 11, $Ni(NO_3)_2$ reacts to soluble hexamminenickel, which is identified by its clear blue color.[34] Thus, an aging step is required to equilibrate at the pH of maximum uptake before the support is added and the adsorption step is performed. Figure 2 shows the results of monitoring Ni^{2+} deposition as a function of pH (adsorption isotherm).

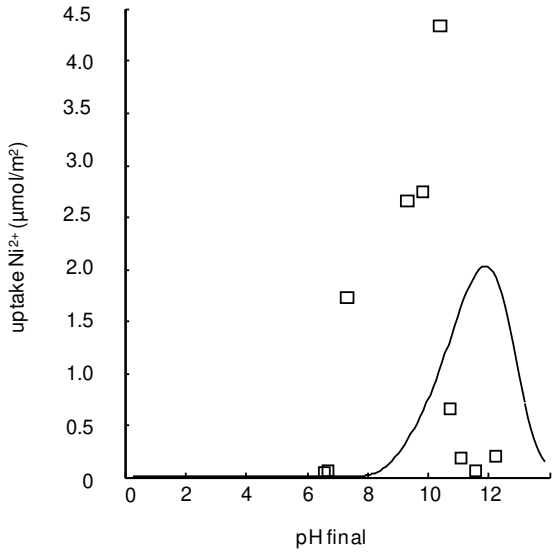

Figure 2 – Nickel nitrate adsorption isotherm and projected uptake based on the revised physical adsorption model. [35] Adjustable theoretical model parameters: Ns = 8 OH/nm^2, difference between pK_1 and pK_2, $\Delta pK = 5$, $r_{ion} = 0.79$ Å, one hydration sheath.[36]

It was attempted to interpret the obtained data using the revised physical adsorption (RPA) model, which is well-established for SEA. [35, 37] Briefly, the model considers only electrostatic (non-specific) interactions between the metal complex and the support to describe adsorption. Two parameters of the model are adjustable: the total number of charged sites N_s and the difference between pK_1 and pK_2 (ΔpK). For alumina, these values can be readily found in literature: $N_s = 8$ OH/nm^2 and $\Delta pK = 5$.[36, 38] The RPA model predicts maximum adsorption to occur in the final pH range of 11.5 to 12.5. However, as previously mentioned, above pH 11, Ni^{2+} forms $Ni(NH_3)_6^{2+}$ which is not accounted for by the RPA model. In addition, it is likely that multiple species in various concentrations exist at the different pH values examined (in an aqueous NH_4OH solution): $Ni(H_2O)_6^{2+}$, $Ni(OH)_2(s)$, and $Ni(H_2O)_{6-n}(NH_3)_n^{2+}$. [39] It has been proposed that certain aquo metal ions (e.g. Pb^{2+}, Co^{2+}, Ni^{2+}) can efficiently penetrate the structured water layers adjacent to the surface and specifically interact with the support

surface,[40] while ammine complexes were found to not specifically adsorb.[41] From Figure 2, it was also observed that non-negligible deposition of nickel occurs near the PZC of γ-Al_2O_3, which also indicates that chemical interactions as well as electrostatic interactions are responsible for the adsorption.[42] The failure of the RPA model to describe adsorption data and the existence of multiple types of nickel species in solution in the presence of NH_4OH indicates that chemical and electrostatic interactions are involved in adsorption of Ni^{2+} on alumina. As a result of the PZC measurements, determination of ranges of bulk precipitation, known solubility limits of alumina,[43] and adsorption isotherm measurements the optimal starting point for the synthesis of 2NiCA was determined to be at an initial pH of 9.5. This value is sufficiently above the PZC of alumina while avoiding bulk precipitation and maximizing adsorption.

3.2 Characterization of 2wt% Ni/Al_2O_3 catalysts prepared by CA and DI

Table 1 shows the results from elemental analysis, N_2 physisorption, and H_2 chemisorption measurements. From elemental analysis, it was found that 2NiCA contained 1.90 wt% nickel and 2NiDI contained 1.98 wt% nickel, respectively. N_2 physisorption was performed on uncalcined, calcined, and reduced samples as well as catalysts after reaction. A small decrease in surface area (relative to fresh alumina) was observed for the uncalcined samples due to the addition of nickel nitrate. Upon calcination, 2NiCA loses 9% of its surface area while 2NiDI loses 30% of its surface area. Catalysts that were reduced at 600 °C for 2 h and subsequently utilized in methane dry reforming at 700 °C for 9 h (post reaction catalysts) both lost an additional 20% of their surface area. Samples that were utilized in TPR experiments were also analyzed by N_2 physisorption. Upon reduction at 1000 °C both samples had a surface area of 55 m^2/g, regardless of the preparation method. Further, the pore volume and the average pore

diameter increased upon precursor deposition and calcination. For 2NiDI the pore volume and pore diameter are found to decrease after exposure to reaction conditions and reduction. For 2NiCA the pore volume is slightly increased after exposure to reaction conditions (presumably due to the presence of filamentous carbon, *vide infra*) and decreased after reduction at 1000 °C. H_2 chemisorption measurements found dispersions of 12.07% for 2NiCA and 0.26% for 2NiDI.

Table 1 – Results from N_2 physisorption, elemental analysis, and H_2 chemisorption of catalysts in different stages of synthesis and after reaction.

Sample	**Surface Area (m^2/g)[a]**	**Pore Volume (cm^3/g)[b]**	**Average Pore Diameter (nm)[c]**	**Elemental Analysis (wt% Ni)[d]**	**Dispersion (%)[d]**
Fresh Alumina	102	0.15	11.7	-	-
Uncalcined 2NiCA	92	0.19	15.0	-	-
Uncalcined 2NiDI	96	0.22	16.1	-	-
Calcined 2NiCA	84	0.17	13.8	1.90	12.07
Calcined 2NiDI	74	0.23	17.5	1.98	0.26
Reacted 2NiCA*	68	0.20	16.2	-	-
Reacted 2NiDI*	60	0.20	16.2	-	-
Reduced 2NiCA**	55	0.14	14.5	-	-
Reduced 2NiDI**	55	0.20	17.4	-	-

[a] Calculated from N_2 physisorption data using the BET equation
[b] Calculated from N_2 physisorption data using the BJH equation applied to the desorption branch of the adsorption isotherm
[c] Calculated from N_2 physisorption data using the BJH equation
[d] Nickel dispersion calculated using H_2 chemisorption data
***Samples reduced at 600 °C for 2 hours prior to 6 h methane dry reforming experiment at 700 °C, 9.5h**
****Samples from TPR, reduced at 5 °C/min to 1000 °C**

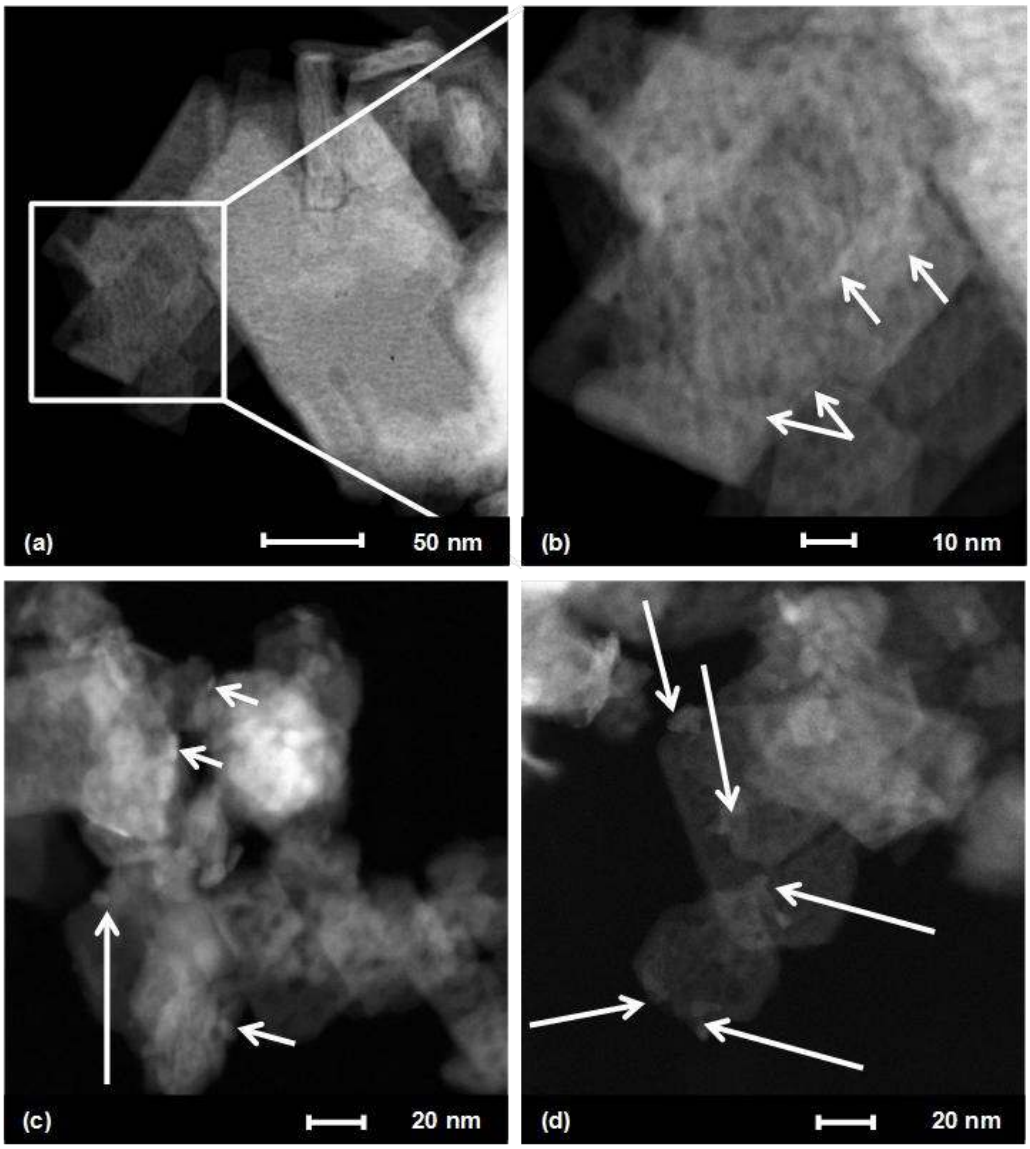

Figure 3 - TEM images (a,b) 2NiDI (c,d) 2NiCA. Arrows point at Ni particles as confirmed by EDS.

TEM images were collected for calcined samples (Figure 3). For 2NiDI, the majority of the TEM images do not clearly reveal any distinguishable particles of Ni containing phases (Figure 3a), and nickel is present on the surface as a very thin layer as indicated by the arrows in Figure 3b. In only one of many collected images for 2NiDI, a NiO particle was observed. The nickel atoms in 2NiDI are suggested to be present close to the surface in the form of a surface

nickel aluminate phase, which has been shown to exhibit weaker contrast as compared to nickel or nickel oxide.[13] For 2NiCA, distinguishable nanoparticles present on the surfaces of γ-Al_2O_3 were identified (Figure 3c,d). Based on high resolution imaging, several of these nanoparticles could be unambiguously identified as $NiAl_2O_4$, while in some other cases lattice spacing analysis points towards NiO. In addition to the presence of NiO and $NiAl_2O_4$ nanoparticles, highly dispersed surface nickel aluminate is present on the surface of γ-Al_2O_3. For 2NiCA, nickel oxide particles of very similar size (~8 nm) and shape were observed in TEM.

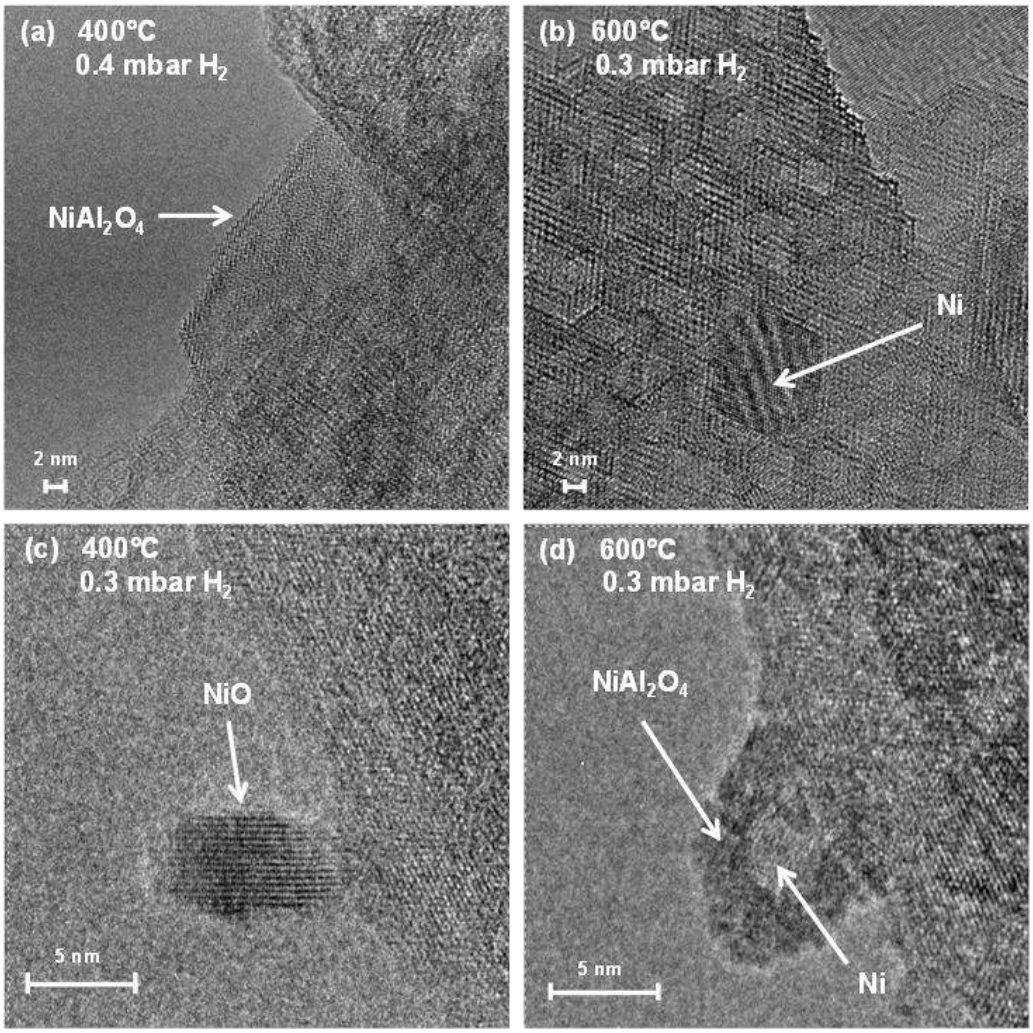

Figure 4 – HRTEM after exposure to the noted temperature and $P(H_2)$ for 30 minutes of 2NiDI (a,b) and 2NiCA (c,d).

Environmental TEM images were obtained for samples exposed to hydrogen at approximate temperatures of 400 and 600 °C to probe the evolution of nickel species during the transition from an oxidized to a reduced state. As with the TEM images obtained after treatment under standard conditions, imaging the 2NiDI sample was extremely difficult due to the weak contrast between $NiAl_2O_4$ and Al_2O_3. However, a $NiAl_2O_4$ phase was observed at a temperature of 400 °C in the presence of hydrogen (Figure 4a). Upon exposure to H_2 at 600°C for 30 minutes, a few moderately sized Ni crystallites (8-10 nm) were observed in 2NiDI (Figure 4b). The particle is likely located on one of the facets of Al_2O_3. Based on the analysis of the lattice fringes, we find that it is epitaxially attached. There is no contrast, which would indicate a presence of encapsulating shell.

In the case of 2NiCA, it was possible to track a single nickel/nickel oxide particle as it was exposed to increasing temperature in the presence of hydrogen. At room temperature and after exposure to H_2 at 400 °C for 30 minutes, the NiO particle had a lamellar structure (Figure 4c). However, once the temperature was increased to 600 °C for 30 minutes, a core shell structure was formed (Figure 4d). Lattice measurements indicate the formation of metallic nickel within a porous $NiO/NiAl_2O_4$ shell. Upon exposure to 0.3 mbar H_2 for 30 minutes at 700 °C, all particles imaged had this core shell structure (Figure 5 a,b). The $NiO/NiAl_2O_4$ overlayer was approximately 2 nm thick in all imaged particles. After exposure to oxygen at 700 °C and prolonged exposure to air at room temperature a hollow core-shell particle was formed (Figure 5 c,d).

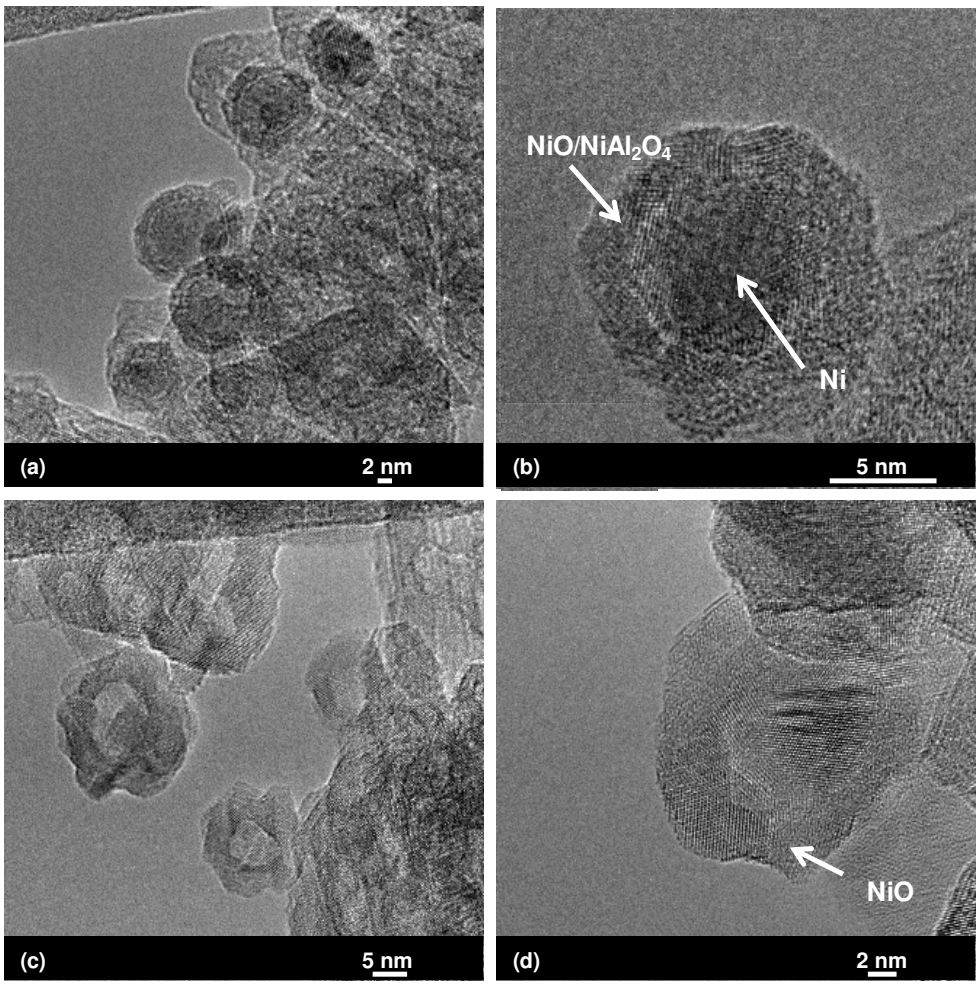

Figure 5 – ETEM of 2NiCA (a,b) after exposure to 0.3 mbar H_2 for 30 minutes at 700 °C (c, d) after previous exposure to H_2 at 700 °C and extend exposure to air at room temperature.

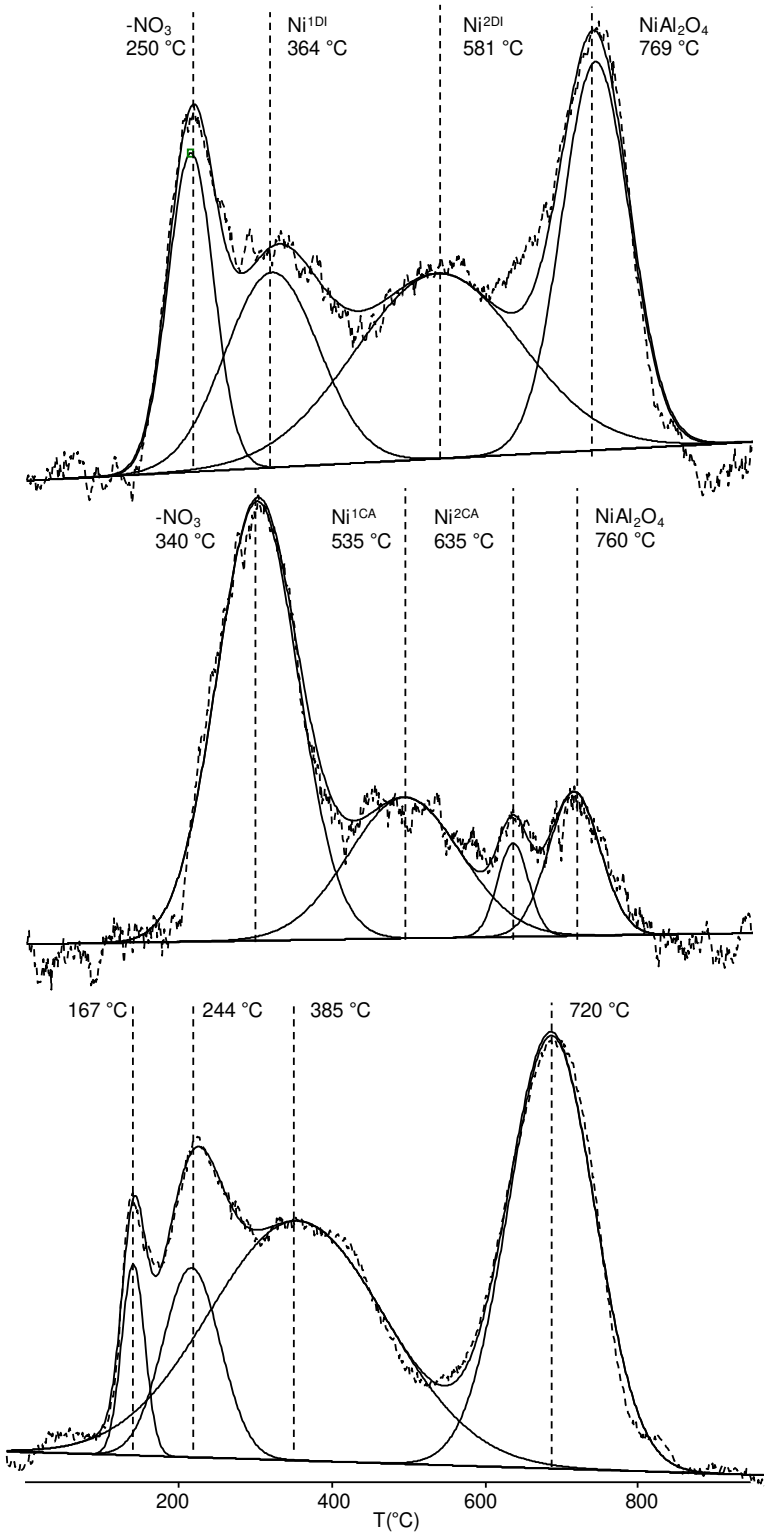

Figure 6 - TPR profiles of (a) 2NiDI and (b) 2NiCA (c) NiCA pretreated in He at 700 °C.

Table 2 – Hydrogen consumption per gram of sample for different TPR peaks based on TCD signal.

Peak Assignment	**Ni^1**	**Ni^2**	**$NiAl_2O_4$**	**Fraction Reduced (%)**
2NiDI $\mu molH_2/ g_{cat}$	124	208	179	75
2NiCA $\mu molH_2/ g_{cat}$	78	14	36	19
2NiCA $\mu molH_2/ g_{cat}$ pretreated in He at 700 °C	N/D	254	224	70

Figure 6 shows the temperature programmed reduction (TPR) profiles obtained for the calcined catalysts, and Table 2 shows the hydrogen consumption of each of the peaks normalized by the mass of catalyst used in the experiment. For the typical TPR experiments (Figure 6a,b), four peaks were deconvoluted from the traces obtained from TPR experiments. The first peak for both samples was attributed to decomposition of residual nitrate.[12, 17] Unsupported $Ni(NO_3)_2 \cdot 6H_2O$ is said to decompose at temperatures lower than 250 °C under flowing air pointing towards a stabilization of the nitrates by the support. [12, 33, 44] This was especially notable in the case of the 2NiCA sample, where the peak was shifted to a higher temperature than the 2NiDI sample. For the first peak, desorption of species other than H_2 is expected (e.g. NO_2, NO, N_2O_5, NH_3, etc.), and, thus, the values of H_2 consumption are omitted because their contribution to the TCD signal cannot be quantified. Additionally, comparison of the relative quantities desorbed between 2NiCA and 2NiDI is not valid because the combination of NO_x gases evolved may be different and cannot be determined with the current experimental set-up. The total hydrogen consumption (excluding the first peak) from TPR corresponds to a total extent of reduction of 75% for 2NiDI and 19% for 2NiCA. For both samples, three distinct peaks

were observed between 300 and 800 °C, which are attributed to different types of nickel species on the alumina surface. The first peak in this region will be designated as Ni^{1*} and the second as Ni^{2*} where the * will designate the preparation method, CA or DI. For 2NiDI prepared samples, Ni^{1DI} and Ni^{2DI} appeared at 364 and 581 °C, respectively. For 2NiCA prepared samples, Ni^{1CA} and Ni^{2CA} appear at 535 and 635 °C, respectively. The 4th peak was observed at 769 °C and 760 °C for 2NiDI and 2NiCA, respectively.

To determine if the extent of reduction could be increased for the 2NiCA sample, the sample was pretreated at 700 °C in helium and cooled prior to the TPR experiment (Figure 6c). Four peaks were observed. Due to the low temperature of the first two peaks (167 °C and 244 °C) it is likely that both of these peaks are due to decomposition of residual nitrates as observed in the case of the other samples. The pretreatment could change the interaction of the nitrates with the support changing the types of nitrate species desorbed and resulting in the appearance of two peaks rather than one. Regardless, the contribution of the first two peaks to the total hydrogen consumption is small. Two peaks attributed to the reduction of nickel type species are observed at 385 °C and 720 °C and the pretreatment results in an increase of the total extent of reduction of 2NiCA to 70%. The exact assignment of these peaks requires careful consideration of different experiments reported in this study (vide infra). The final peak in the TPR profiles of all samples appeared at 720-770 °C and was assigned to the reduction of nickel present in a spinel phase.[12]

3.3 Reactivity Studies

The initial methane conversion was 83% for 2NiDI and 91% for 2NiCA, respectively (Figure 7). For 2NiCA, the methane conversion increased to 98%, while 2NiDI deactivated

slightly to 80% over the 9 hours examined (Figure 7a). Both samples initially converted 70% of the carbon dioxide (Figure 7b). Over the time examined, 2NiDI deactivated to 60% carbon dioxide conversion and 2NiCA to 49%. For both catalysts, the H_2/CO ratio was less than unity indicating that the inverse water gas shift reaction contributed to the product mixture (Figure 7c).[45] The conversion relative to the moles of nickel present in each sample is termed specific activity (Figure 7d).

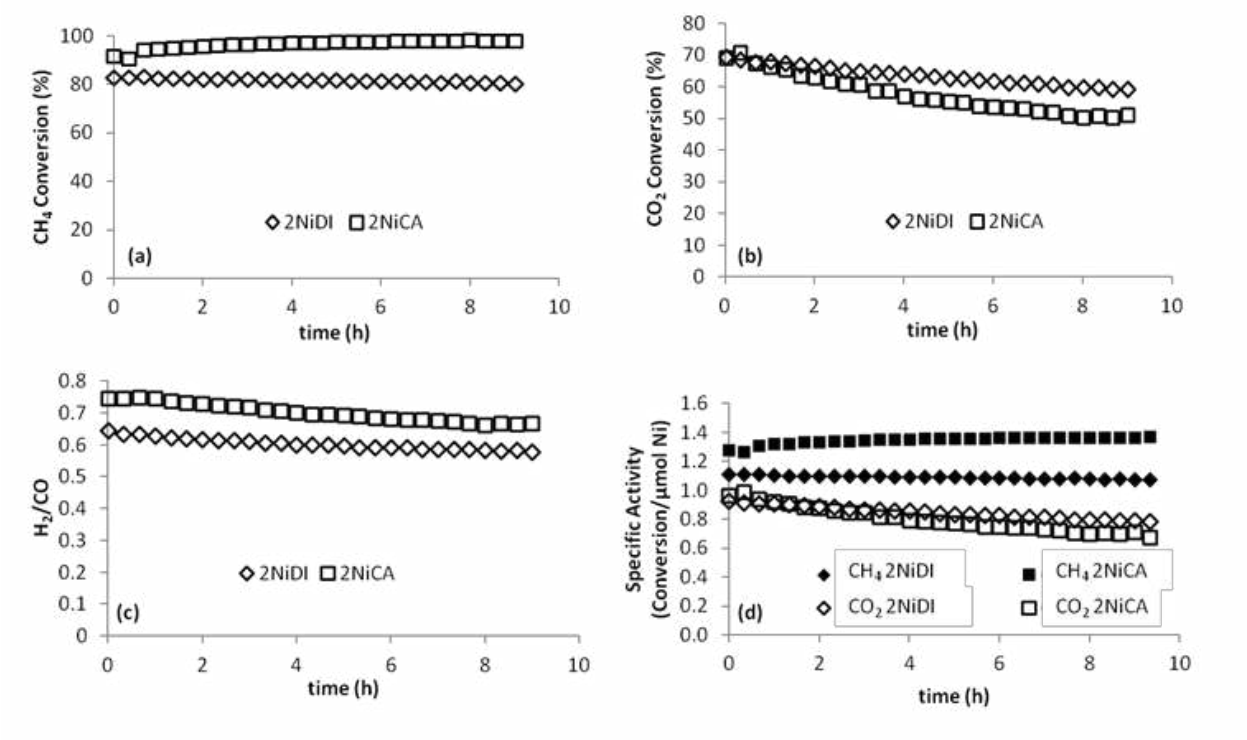

Figure 7 – Methane dry reforming studies using CH_4:CO_2 = 1, 700 °C, and 1.5 atm over 9.0 h. Catalysts pre-reduced at 600 °C for 2 h. (a) Conversion of methane (b) Conversion of carbon dioxide (c) Hydrogen to carbon monoxide ratio (d) Specific activity (Conversion/µmol Ni).

Combustion analysis of spent catalysts showed that 2NiCA contained 16.7 wt% carbon, whereas 3.6 wt% of carbon were found on 2NiDI. Both samples were found to have less than

0.05 wt% hydrogen and nitrogen, respectively. XPS was used to probe the different types of carbonaceous deposits (Figure 8). The C1s scan was performed on two different spots for each sample and the results were averaged.

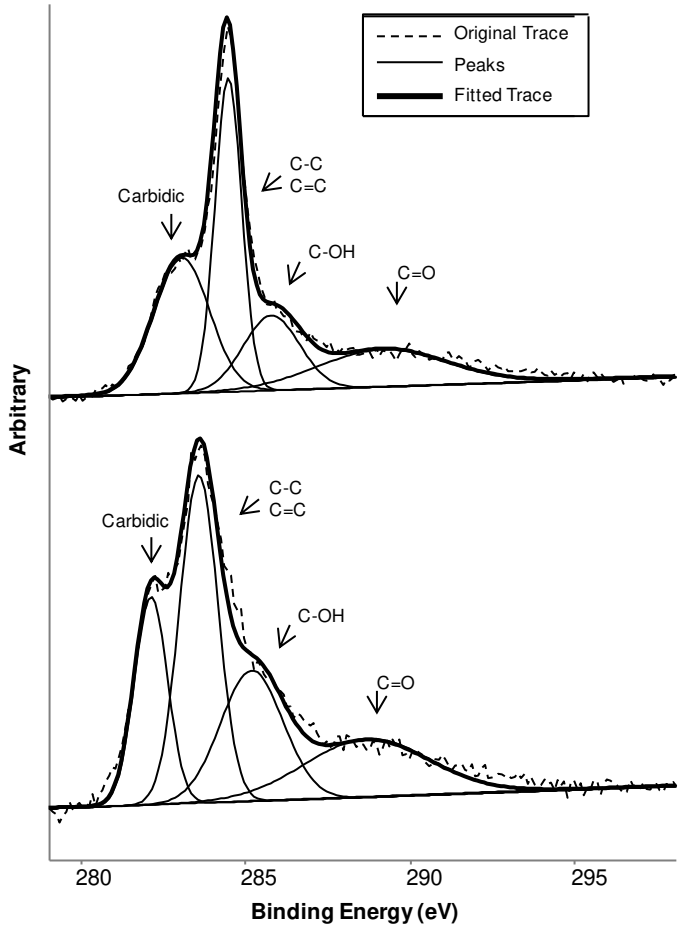

Figure 8 - X-ray photoelectron spectra in the C1s region of catalysts after 9 h methane dry reforming reaction (a) 2NiDI (b) 2NiCA.

The C1s spectrum was deconvoluted to reveal the types of carbonaceous species.[46] The peaks are assigned to carbidic carbon (BE 282.1 – 283.1 eV), graphitic carbon (BE 283.6-284.5 eV), carbon present in alcohol or ether groups (285.2 – 285.8 eV), and carbon present in

carbonyl groups (BE 288.7 – 289.2 eV), respectively. Carbon present as alcohol, ether, or carbonyl groups are referred to as oxidic carbon and the species were present in the same proportion in each sample. The ratios of the types of carbidic: graphitic: oxidic carbon were 0.8: 0.9: 1 for 2NiDI and 0.5: 0.8: 1 for 2NiCA.

4 Discussion

4.1 Nickel Speciation

NiO is generally considered to exist in two forms, free (Figure 1 a,b) and fixed (Figure 1 c,d).[19] Free refers to nickel that exists on the catalyst surface as nickel oxide, while fixed nickel oxide originates from a chemical reaction between alumina and nickel oxide forming stoichiometric and non-stoichiometric nickel aluminate ($NiAl_2O_4$). The assignment of nickel species present on an alumina surface derived from TPR has been discussed extensively in the literature. Scheffer et al. investigated the effect of the calcination temperature on nickel catalysts with metal contents prepared by dry impregnation.[12] For a 1.6 wt% Ni/Al_2O_3 catalyst that was calcined at 400 °C, the TPR peaks were assigned as follows: 427 – 627 °C: reduction of disperse nickel oxide interacting with the support, and between 747 – 877 °C: reduction of "a surface nickel species". The general assignment of "a surface nickel species" was used because it was thought that a calcination temperature of 400 °C was too low to form spinel species. When the calcination temperature was increased to 650 °C, the peak in the region of 747 – 877 °C became sharper and was assigned to a diluted $NiAl_2O_4$ like phase formed by diffusion of nickel ions into the support. Zhang et al. investigated the effect of the calcination temperature on nickel species. [24] In their study, the alumina support was calcined at 600 °C prior to impregnation with nickel. For a sample with 2 wt% nickel, only one peak, at 527 °C, was observed in the temperature range

of interest (25 – 727 °C), and it was attributed to reduction of surface nickel aluminate. Rynkoswki et al. examined 5 wt% Ni/Al_2O_3 prepared by dry impregnation. They observed a peak at 500 °C, which they attributed to the reduction of an amorphous overlayer of NiO, and a shoulder at 750 °C was said to be connected with the reduction of non-stoichiometric, spinel type Ni-Al oxides.[10, 17] Zielinski investigated the effect of nickel loading in Ni/Al_2O_3 prepared by impregnation followed by calcination at 400 °C.[19] For the sample with 2 wt% nickel, only one reduction peak was observed at 500 °C, and it was attributed to $NiAl_2O_4$.

Due to the significant disparity of assignments of TPR traces for nickel catalysts in literature, a combination of results from literature and complimentary experiments from the present study must be used to adequately identify the types of nickel species as a function of deposition method and thermal treatment procedure. In this context, it is important to carefully consider experimental procedures utilized in each experiment. Prior to chemisorption, the samples were reduced at 600 °C for 8 h and evacuated at 550 °C for 16 h. Then, H_2 was dosed at 25 °C to determine dispersion. Using this method, the measured dispersion was 0.26% and 12.1% for 2NiDI and 2NiCA, respectively. The low value of dispersion reported for 2NiDI is not unusual.[21, 24, 47] Huang and Schwarz reported that the suppression of hydrogen uptake after high temperature reduction was due to coverage of nickel crystallites by Al_xO_y moieties, which is facilitated when adsorbed surface species are removed from nickel particles in vacuum or under inert gas.[21] Zhang et al. proposed that poor reducibility was due to diffusion of Ni^{2+} ions into the alumina lattice near the surface during spreading of Al_xO_y moieties. Al^{3+} ions counter diffuse to the surface of NiO crystallites producing covered NiO crystallites on the surface.[24]

In the case of 2NiDI, it is speculated that weak metal support interactions allow diffusion of Ni^{2+} ions into the alumina lattice during calcination resulting in the formation of $NiAl_2O_4$ [48].

The formation of this phase occurs when Al^{3+} cations migrate from octahedral to tetrahedral sites.[49] Nickel preferentially occupies newly vacant octahedral sites in the transient alumina phase.[50] In agreement with this interpretation, studies regarding the influence of cationic additives (e.g. $Mg^{2+,}$ $Ca^{2+,}$ Ni^{2+}, etc.) on the stability of alumina found that Ni^{2+} has little or no effect on impeding the phase transformation of gamma alumina.[51] N_2 physisorption measurements indicated that the phase transformations in 2NiDI during calcination resulted in a significant loss of surface area (*ca.* 30%). TEM measurements performed after calcination further confirmed that Ni primarily exists as a surface $NiAl_2O_4$ layer. ETEM measurements revealed the presence of few free nickel particles. However, the majority of TEM and ETEM images show weak contrast indicating nickel was primarily present as a thin, disperse layer of surface $NiAl_2O_4$ after calcination and prior to TPR measurements. Consequently, the mid-range peaks in the TPR profiles of 2NiDI, Ni^{1DI} and Ni^{2DI}, are assigned to the reduction of surface $NiAl_2O_4$ (small, fixed NiO) that interacts weakly and strongly with the support, respectively. The fourth peak in the TPR profile was attributed to reduction of the $NiAl_2O_4$ in the bulk. Quantification of H_2 consumed during TPR correlates to nearly 75% reduction of the nickel present in the sample. The high extent of reduction in TPR experiments as compared to H_2 chemisorption measurements is explained by considering the differences in the experimental techniques. During TPR measurements and in the preparation of the sample for chemisorption measurements, surface $NiAl_2O_4$ phases present in different forms on the catalyst are reduced to non-stoichiometric oxides ($Ni+Al_2O_3$).[19] In dispersion measurements, after reduction, hydrogen was pulsed onto the sample, and nickel present as $Ni+Al_2O_3$ was not available for H_2 chemisorption. We speculate that the metallic particles formed during reduction are embedded in the aluminate structure and not available for hydrogen chemisorption.[52]

The relatively high dispersion obtained for 2NiCA shows that strong metal support interactions can suppress the diffusion of Ni^{2+} into the γ-Al_2O_3 lattice at mild conditions, which has also been observed in other studies on nickel-alumina catalysts.[25, 48] Under the experimental conditions utilized in chemisorption measurements it is likely that a significant fraction of nickel exists as small, free nickel particles as indicated by the ETEM measurements. When 2NiCA is heated in H_2 at 600 °C there is a high density of core-shell particles that suddenly appear suggesting that before exposure to reducing conditions, free NiO was dispersed in higher proportion than $NiO/NiAl_2O_4$ surface layer. Upon exposure to reducing conditions at 700 °C the majority of the nickel species become covered by nickel aluminate surface layer similar to the transformation observed by Lamber et al. [13] Therefore, Ni^{1CA} in the TPR profile is attributed to reduction of small (free) NiO as indicated by the high temperature of the peak, and dispersion and ETEM results. The high temperatures of Ni^{1CA} indicated, as expected for this preparation method, that 2NiCA has strong metal support interactions. The low extent of reduction during TPR for 2NiCA can be understood by considering N_2 physisorption and ETEM results. Surface area analysis of 2NiCA after TPR measurements (up to 1000 °C) indicated a 35% loss in surface area, which could point to an increased formation of surface nickel aluminate. The ETEM results clearly showed that at 600 °C (in the presence of hydrogen) Ni crystallites become encapsulated in a $NiO/NiAl_2O_4$ shell. Interestingly, reduced samples from ETEM measurements were re-oxidized and formed hollow core-shell structures upon exposure to oxygen at 700 °C for 30 minutes and extended exposure to air at room temperature. Formation of these hollow shell structures is consistent with the Kirkendall effect where nickel is found to diffuse faster through than oxygen through the porous $NiO/NiAl_2O_4$ overlayer,[53] providing further confirmation of a metallic core existing under the overlayers under high temperature

reduction conditions. A temperature of 600 °C appears to be an approximate threshold for the transformation of Ni species in the 2NiCA sample as this was the temperature utilized for reduction before performing H_2 chemisorption, which indicated a relatively high dispersion. Thus, the low total degree of reduction obtained during TPR can be attributed to transient aluminate shell formation. This transient behavior of 2NiCA is confirmed by the modified TPR experiment where 2NiCA was heated to 700 °C in helium prior to performing the TPR. Unfortunately, it was impossible to determine if the same aluminate overlayers were formed in helium as were observed in ETEM under hydrogen due to experimental constraints of the MEMS chip. However, it is clear that the low extent of reduction obtained in the conventional TPR is the result of transient formation of nickel species at high temperatures, which is prevented when the sample is aged under inert gas. Thus, the Ni^{2CA} peak is assigned to reduction of NiO or surface $NiAl_2O_4$ layers, which strongly interact with their environment. Due to the formation of overlayers the reduction of these species remains limited unless an aging step is implemented. The fourth peak at approximately 760 °C was attributed to reduction of the $NiAl_2O_4$ surface layer (observed in TEM).[19]

4.2 Catalytic Performance and Deactivation

The effect of different types of nickel species on catalytic activity and the formation of carbonaceous deposits was illustrated by the performance of 2NiDI and 2NiCA in methane dry reforming experiments that were conducted for 9.0 hours at 700 °C using a stoichiometric feed of carbon dioxide and methane. The desired reaction is (1),[54]

$$CH_4 + CO_2 \leftrightarrow 2CO + 2H_2 \quad \Delta H^0_{298K} = 247 \text{ kJ/mol} \quad (1)$$

Inverse water-gas shift (2), methane steam reforming (3), and deposition of carbonaceous deposits (4, 5) are also known to occur during methane dry reforming,

$$CO_2 + H_2 \leftrightarrow 2CO + H_2O \quad \Delta H^0_{298K} = 41 \text{ kJ/mol} \quad (2)$$

$$CH_4 + H_2O \leftrightarrow CO + 3H_2 \quad \Delta H^0_{298K} = 206 \text{ kJ/mol} \quad (3)$$

$$CH_4 \rightarrow C + 2H_2 \quad \Delta H^0_{298K} = 75 \text{ kJ/mol} \quad (4)$$

$$2CO \rightarrow C + CO_2 \quad \Delta H^0_{298K} = -171 \text{ kJ/mol} \quad (5)$$

Nickel alumina catalysts have been widely investigated for the dry reforming of methane.[55] Guo et al. studied a 10 wt% Ni/Al_2O_3 catalyst prepared by wet impregnation.[56] At 750 °C, the conversion of methane was 61% CH_4, and the conversion of CO_2 was 63%. Over the course of 12 h on stream, the conversions of methane and carbon dioxide decreased to 32% and 30%, respectively. San Jose et al. studied 9 wt% Ni/Al_2O_3 prepared by wet impregnation for methane dry reforming at 700 °C and atmospheric pressure.[4] The conversion of methane was initially 63% and decreased to 55% after 6 h on stream. Wang et al. examined the effect of nickel precursor on activity of 8 wt% Ni/Al_2O_3 catalysts. At 700 °C between 70-80 % of methane and carbon dioxide were converted depending on the nickel precursor used to synthesize the catalyst.[57]

The catalysts used in this study had a lower nickel content (2 wt%) than the ones used in the previous studies mentioned above. Nevertheless they provide higher activity and slower deactivation durig dry reforming of methane at 700 °C. Specifically, the initial methane conversion was 91% for 2NiCA, and it increased to 98% over the 9 hours examined. In the case of 2NiDI, an initial methane conversion of 83% was found, which decreased to 80% over 9 h on stream.

One would expect that, because of the low apparent dispersion obtained from H_2 chemisorption, 2NiDI would not have performed as well in the methane dry reforming studies as was observed. Based on assignments of the types of nickel species that exist on the catalyst surface, it seems reasonable that under reaction conditions surface $NiAl_2O_4$ identified in 2NiDI must be catalytically active.[58, 59] In the beginning of the reaction, 2NiCA likely contained a mixture of small, free nickel particles as well as nickel particles encapsulated by porous $NiO/NiAl_2O_4$ overlayer. The types of active sites on 2NiCA could evolve dynamically as the reaction progresses. On a specific basis, both catalysts converted similar amounts of carbon dioxide, and 2NiCA had a higher H_2/CO ratio confirming that the types of sites affect activity and selectivity of the methane dry reforming reaction favoring different reaction pathways. It was shown that different surface nickel species exhibit different catalytic behavior, such as activity and mechanism for methanation of CO.[20] The higher H_2/CO ratio for 2NiCA and the increase in methane conversion indicated that this catalyst could promote steam reforming of methane (reaction 3) more effectively than 2NiDI (Figure 7c). The relative rate of carbon deposition is negligible compared to the change of methane concentration indicating coking is not the primary reason for the observed increase in methane conversion. Further, if one analyzes the conversion relative to the moles of nickel present in the sample (specific activity), it can be seen that the 2NiCA sample uses the metal present more effectively than 2NiDI (Figure 7d). Deactivation of these catalysts over the time period examined was minimal relative to our previous study where cobalt on alumina catalysts were studied for the methane dry reforming reaction.[33]

The quantity and types of carbonaceous deposits are explained by considering nickel speciation. Spent samples differ primarily in the amount of carbidic carbon with 2NiDI having

nearly twice the amount of carbidic carbon. Aluminate species have been said to propagate the formation of carbidic carbon, explaining why there was a larger amount of that type of carbonaceous deposit in 2NiDI.[33] Further, the total amount of carbon deposited on 2NiDI is four times less than that deposited on 2NiCA indicating gasification of carbonaceous deposits is more easily accomplished on dispersed surface $NiAl_2O_4$.

5 Conclusions

Preparation methods drastically affect the type of nickel species present on alumina supported nickel catalyst. In the case of samples prepared by controlled adsorption (2NiCA), where the preparation method induces strong metal support interactions, the formation of nickel aluminate is reduced at mild conditions. However, once the temperature is increased beyond 600 °C the thermal energy of the system is great enough to overcome the 5 – 15 kJ/mol energy of metal-support bond,[48] and the formation of aluminates cannot be entirely avoided as indicated by physiochemical characterization results. In the case of nickel samples prepared by dry impregnation (2NiDI), H_2 chemisorption results indicated low dispersion, and considering TPR, ETEM, and reactivity measurements, it is concluded that surface $NiAl_2O_4$ is the primary type of nickel species. The sample prepared by controlled adsorption (2NiCA) is found to have a higher dispersion from H_2 chemisorption, and the free nickel oxide particles are found to be covered by nickel aluminate surface layers at temperatures in excess of 600 °C as indicated by the decline in H_2 consumption during TPR measurements. The formation of these core shell structures is confirmed by ETEM. Low weight loading nickel alumina catalysts were found to have excellent activity and stability for methane dry reforming. The types of active sites present affect the selectivity, activity, and carbonaceous deposits of the catalysts.

Further, there is a broader implication of this work. Through careful preparation of catalysts and characterization at each step in preparation/treatment a template has been outlined to tailor types of nickel sites on γ-Al_2O_3 surface to be used in a wide range of reactions.

Acknowledgements

The authors wish to thank Micromeritics Corporation and Jeff Kenvin for TPR and H_2 chemisorption measurements. Funding from The Dow Chemical Company and the Renewable Bioproducts Institute at the Georgia Institute of Technology is gratefully acknowledged. Transmission Electron Microscopy measurements described in this paper were conducted in the William R. Wiley Environmental Molecular Sciences Laboratory (EMSL), a national scientific user facility sponsored by DOE's Office of Biological and Environmental Research and located at Pacific Northwest National Laboratory.

References

[1] E. Ruckenstein, Y.H. Hu, J. Catal. 162 (1996) 230-238.
[2] N. Salhi, C. Petit, A. Kiennemann, in: A. Gedeon, P. Massiani, F. Babonneau (Eds.), Zeolites and Related Materials: Trends, Targets and Challenges, Proceedings of the 4th International Feza Conference, 2008, pp. 1335-1338.
[3] S.Y. Foo, C.K. Cheng, T.H. Nguyen, A.A. Adesina, J. Mol. Catal. A: Chem. 344 (2011) 28-36.
[4] D. San-Jose-Alonso, J. Juan-Juan, M.J. Illan-Gomez, M.C. Roman-Martinez, Appl. Catal. A: Gen. 371 (2009) 54-59.
[5] M.M. Yung, W.S. Jablonski, K.A. Magrini-Bair, Energy Fuels. 23 (2009) 1874-1887.
[6] D. Sutton, B. Kelleher, J.R.H. Ross, Fuel Process. Technol. 73 (2001) 155-173.
[7] A. Winkler, H. Borchert, K. Al-Shamery, Surf. Sci. 600 (2006) 3036-3044.
[8] C.H. Bartholomew, R.J. Farrauto, J. Catal. 45 (1976) 41-53.
[9] Y.J. Huang, J.A. Schwarz, Appl. Catal. 30 (1987) 239-253.
[10] J.M. Rynkowski, T. Paryjczak, M. Lenik, Appl. Catal. A: Gen. 126 (1995) 257-271.
[11] Y.J. Huang, J.A. Schwarz, J.R. Diehl, J.P. Baltrus, Appl. Catal. 36 (1988) 163-175.
[12] B. Scheffer, P. Molhoek, J.A. Moulijn, Appl. Catal. 46 (1989) 11-30.
[13] R. Lamber, G. Schulzekloff, Surf. Sci. 258 (1991) 107-118.
[14] J. Hu, J.A. Schwarz, Y.J. Huang, Appl. Catal. 51 (1989) 223-233.
[15] K.V.R. Chary, P.V.R. Rao, V.V. Rao, Catal. Commun. 9 (2008) 886-893.
[16] C.P. Li, Y.W. Chen, Thermochimica Acta. 256 (1995) 457-465.
[17] J.M. Rynkowski, T. Paryjczak, M. Lenik, Appl. Catal. A: Gen. 106 (1993) 73-82.
[18] P. Salagre, J.L.G. Fierro, F. Medina, J.E. Sueiras, J. Mol. Catal. A: Chem. 106 (1996) 125-134.
[19] J. Zielinski, J. Catal. 76 (1982) 157-163.
[20] Y.J. Huang, J.A. Schwarz, Appl. Catal. 36 (1988) 177-188.
[21] Y.J. Huang, J.A. Schwarz, J.R. Diehl, J.P. Baltrus, Appl. Catal. 37 (1988) 229-245.
[22] M. Lojacono, Schiavel.M, A. Cimino, J. Phys. Chem. 75 (1971) 1044-&.
[23] N. Sahli, C. Petit, A.C. Roger, A. Kiennemann, S. Libs, M.M. Bettahar, Catal. Today. 113 (2006) 187-193.
[24] L.F. Zhang, J.F. Lin, C. Yi, J. Chem. Soc. Faraday Trans. 88 (1992) 497-502.
[25] A. Gil, A. Diaz, L.M. Gandia, M. Montes, Appl. Catal. A: Gen. 109 (1994) 167-179.
[26] R. Lamber, G. Schulzekloff, J. Catal. 146 (1994) 601-607.
[27] D.S. Jose-Alonso, M.J. Illan-Gomez, M.C. Roman-Martinez, Int. J. Hydrog. Energy. 38 (2013) 2230-2239.
[28] L. Jiao, J.R. Regalbuto, J. Catal. 260 (2008) 329-341.
[29] L. Jiao, J.R. Regalbuto, J. Catal. 260 (2008) 342-350.
[30] R.R. John, Catalyst Preparation, CRC Press, 2006, pp. 297-318.
[31] K.P.d. Jong, Synthesis of Solid Catalysts, Wiley, Utrecht, 2009.
[32] K.S.W. Sing, D.H. Everett, R.A.W. Haul, L. Moscou, R.A. Pierotti, J. Rouquerol, T. Siemieniewska, Pure Appl. Chem. 57 (1985) 603-619.
[33] J.L. Ewbank, L. Kovarik, C.C. Kenvin, C. Sievers, Green Chem. 16 (2014) 885-896.
[34] Holleman-Wiberg, Inorganic Chemistry, Academic Press, 2001.
[35] M. Schreier, J.R. Regalbuto, J. Catal. 225 (2004) 190-202.

[36] J.A. Schwarz, Contescu, C., Surfaces of Nanoparticles And Porous Materials, Ipswich, MA, 1999.
[37] J.R. Regalbuto, A. Navada, S. Shadid, M.L. Bricker, Q. Chen, J. Catal. 184 (1999) 335-348.
[38] X. Hao, W.A. Spieker, J.R. Regalbuto, J. Colloid Interface Sci. 267 (2003) 259-264.
[39] A.J. van Dillen, R. Terorde, D.J. Lensveld, J.W. Geus, K.P. de Jong, J. Catal. 216 (2003) 257-264.
[40] W. Stumm, H. Hohl, F. Dalang, Croat. Chem. Acta. 48 (1976) 491-504.
[41] D.W. Fuerstenau, K. Osseoasare, J. Colloid Interface Sci. 118 (1987) 524-542.
[42] K. Bourikas, C. Kordulis, J. Vakros, A. Lycourghiotis, Adv. Colloid Interface Sci. 110 (2004) 97-120.
[43] S.L. Chen, H.L. Zhang, J. Hu, C. Contescu, J.A. Schwarz, Appl. Catal. 73 (1991) 289-312.
[44] M.A.A. Elmasry, A. Gaber, E.M.H. Khater, J. Therm. Thermal Analysis and Calorim. 52 (1998) 489-495.
[45] M.K. Nikoo, N.A.S. Amin, Fuel Process. Technol. 92 (2011) 678-691.
[46] J.W. Long, M. Laskoski, G.W. Peterson, T.M. Keller, K.A. Pettigrew, B.J. Schindler, J. Mater. Chem. 21 (2011) 3477-3484.
[47] W.J. Wang, Y.W. Chen, Appl. Catal. 77 (1991) 223-233.
[48] J. Lif, M. Skoglundh, L. Lowendahl, Appl. Catal. A: Gen. 228 (2002) 145-154.
[49] X. Krokidis, P. Raybaud, A.E. Gobichon, B. Rebours, P. Euzen, H. Toulhoat, J. Phys. Chem. B. 105 (2001) 5121-5130.
[50] W.L. Chu, W.S. Yang, L.W. Lin, Appl. Catal. A: Gen. 235 (2002) 39-45.
[51] P. Burtin, J.P. Brunelle, M. Pijolat, M. Soustelle, Appl. Catal. 34 (1987) 225-238.
[52] B.C. Enger, R. Lodeng, J. Walmsley, A. Holmen, Appl. Catal. A: Gen. 383 (2010) 119-127.
[53] S. Chenna, P.A. Crozier, Micron. 43 (2012) 1188-1194.
[54] J.G. Zhang, H. Wang, A.K. Dalai, J. Catal. 249 (2007) 300-310.
[55] S.B. Wang, G.Q.M. Lu, G.J. Millar, Energy & Fuels. 10 (1996) 896-904.
[56] J.J. Guo, H. Lou, H. Zhao, D.F. Chai, X.M. Zheng, Appl. Catal. A: Gen. 273 (2004) 75-82.
[57] S.B. Wang, G.Q. Lu, Appl. Catal. A: Gen. 169 (1998) 271-280.
[58] A. Alubaid, E.E. Wolf, Appl. Catal. 40 (1988) 73-85.
[59] J.R.H. Ross, M.C.F. Steel, A. Zeiniisfahani, J. Catal. 52 (1978) 280-290.